DT#48197 QA:NA CB 7/5/06

THE EFFECT OF TEMPERATURE ON THE BREAKDOWN AND REPASSIVATION POTENTIALS OF WELDED ALLOY 22 IN 5 M $CaCl_2$

G. O. Ilevbare

Lawrence Livermore National Laboratory

7000 East Ave, L-631, Livermore CA 94550, USA

ABSTRACT

The study of the electrochemical behavior of wrought and welded Alloy 22 was carried out in 5 M $CaCl_2$ as a function of temperatures between 45 and 120 °C with Multiple Crevice Assembly (MCA) specimens. The susceptibility to corrosion was found to increase with increase in electrolyte temperature in both the wrought (in the mill annealed condition) and the welded forms of the alloy. The weld metal was found to be less susceptible to localized corrosion under the conditions tested.

Keywords: Alloy 22, welds, wrought, mill annealed, gas tungsten arc weld (GTAW), multiple crevice assembly (MCA), localized corrosion, crevice corrosion, localized corrosion resistance, corrosion potential, crevice breakdown potential, crevice repassivation potential, cyclic polarization, 5 M $CaCl_2$, chloride, temperature.

INTRODUCTION

Alloy 22 (UNS number N06022) is a nickel alloy rich in chromium (Cr) and molybdenum (Mo), with a high degree of corrosion resistance. It exhibits a low general corrosion rate under most conditions and has formidable localized and general corrosion resistance in most environments [1-8].

Although the welds generally constitute a very small portion of the total surface area of a component, welds are generally thought to be weak points, and thus favorable sites for localized corrosion initiation [9-22]. The different zones in welds are microstructurally distinct from one another and from the base metal [11, 13-18, 20-23] and make welds and heat affected zones more susceptible to corrosion. For instance, microsegregation of Mo in the dendritic/interdendritic area [13-15, 24, 25] results in Mo enrichment in the interdentritic zones thus significantly depleting Mo (and to some extent Cr) in the adjacent areas especially the dendritic zone. This causes preferential attack of the dendrites.

The use of overmatched (more highly alloyed) filler metal instead of autogenous welds usually results in reducing the effects of microsegregation [12-14, 16]. For instance, increasing the amount of alloyed Mo mitigates the effects of microsegregation, although this might occasionally result in galvanic couples between the more noble welds and less noble base metal [13, 15, 16, 26]. Consequently, welds of highly alloyed Ni-alloys like 625 and Alloy 22 tend to suffer less from the effect of microsegregation compared with more lightly alloyed Ni-alloys and stainless steels.

The behavior of welds is complicated and often difficult to predict because of the distinct microstructure present in different areas of the weld and heat affected zones created by the welding process, including the presence of secondary phase and carbide precipitates[1] [11, 13-18, 20-23]. There are reported cases of welds on Ni-alloys, steels and other alloys exhibiting the same or superior corrosion resistance compared with that of the base metal, and other instances in which welds behaved in an unpredictable manner displaying areas of both superior and inferior corrosion resistance compared with the base metal [10, 13, 26]. Ultimately, the behavior of the weld is dependent on many factors and never really known until it has been characterized in the service environment. It is therefore important to fully characterize and understand the electrochemical behavior of the welds to be used in waste container fabrication.. A comparison of the degree of susceptibility to corrosion of the welded zones and the areas adjacent to the welded zones, with the non-welded portions is therefore necessary to as a preliminary step to assess possible container failure from the corrosion of welds.

Crevice corrosion of Alloy 22 is a concern in Cl^- environments [2-4]. The study of the crevice corrosion behavior of Alloy 22 in the wrought and welded forms has been carried out in 5 M $CaCl_2$ as a function of temperature using a multiple crevice assembly (MCA) specimen configuration. These experiments constitute very preliminary findings from potentiodyanmic experiments intended as a fast screening method of the resultant welds. As such they do not include in-depth experimentation with specimens of pure weld metal, and pure heat affected zone metal. Further, data identifying the composition of the specific secondary phase precipitates and carbides formed during GTAW welding in Alloy 22 were not collected. Also, no experiments to

[1] For Alloy 22 and Ni- Alloys these compounds include μ-phase intermetallic compound $Ni_{17}Mo_6$, and the Mo_6C carbide, Laves, η and σ phases. [20]. Specifically, the σ, μ and P phases in found in Alloy 22 are often referred to as TCP (Tetrahedral Close Packed) phases [25]. Laves phases have the composition AB_2, where the A atoms are ordered as in diamond, hexagonal diamond, or a related structure, and the B atoms form tetrahedra around the A atoms [27].

quantify the effects of each of the secondary phase precipitates and carbides on corrosion resistance were carried out, and as such, any analyses in that regard is beyond the scope of this manuscript and are not addressed herein.

These manuscript reports in detail the observations of experiments performed in 5 M $CaCl_2$ as a function of temperature. It should be noted that these experiments compare the corrosion susceptibilities of the base and weld metal as they would be present under service conditions. It is by no means an exercise in predicting long term behavior of weld and base metal under long term applications and should never be used as such.

5 M $CaCl_2$ was selected because of its very high Cl^- concentration, for use to probe the depths of susceptibility of Alloy 22 to localized corrosion in a series of fast experiments. The MCA configuration used in this work is optimized for the study of crevice corrosion as it provides 24 potential crevice generation sites on a surface area of less than 10 cm^2. The temperature range of study was between 45 and 120 °C (±2 °C).

EXPERIMENTAL PROCEDURE

The material used in this study is Alloy 22 (N06022). The chemical compositions of the plates as well as that of the filler metal (wire) used in the welding process appear in Table 1 as documented by the supplier. The composition of the filler metal was analyzed for before it was used in the welding process (Table 1). The compositions of the plates and filler metal are consistent with ASTM-B 574 and ASTM-B 575 standards for rods (wires) and plates/sheets respectively [28, 29]. The weld metal also meets the standard of ASME SFA5.14 for

ERNiCrMo-10 (F number 43), which is for the matching filler metal for Alloy 22. The composition of the filler metal was taken before it was used in the welding process. Since the compositions of the wrought and filler metal used for the specimens are very similar (Table 1), the expectation is that the nominal composition of the final weld metal would be similar to that of the weld filler metal and wrought portions of the specimens (Table 1). No analyses of the final weld metal was carried out because there was a concern that reporting weld composition derived from local (raster) area(s) of the weld would be misleading because of local compositional variations.

Only Multiple Crevice Assembly (MCA) specimens were used in this work. MCA specimens (Figure 1) containing pure wrought (in the mill annealed condition), as well as those containing both the wrought and weld metal (in the as welded condition) were fabricated for these experiments. The MCA specimens look like lollipops (Figure 1). The wrought specimens were made from ~2 mm thick plates, while the welded specimens were made from 3.175 cm (1.25 inch) thick plates. The design of the MCA specimen was optimized for the study of crevice corrosion so that most of the working surface was covered by the ceramic crevice former after it was fully assembled with the ceramic washers and other hardware components. The working surfaces of the MCA specimens were used in the as-received state after degreasing with acetone and methanol. In the as-received state, the working surfaces of the MCA specimens were finished to a root mean square (RMS) roughness average (RA) of between 2 and 5 micro inches by the manufacturer and had an air formed oxide film. No other surface finishing was applied to the surface prior to experimentation. The edge (surface 90 degrees in angle to the working surface) of the specimens was finished with 600-grit SiC paper after first grinding with 100 and then 240-grit paper to remove damage done to them by the electric discharge machine (EDM) used during specimen fabrication. The welded MCA specimens were identical to the wrought

specimens in configuration. The welds in the specimens were made by means of Gas Tungsten Arc Welding (GTAW). The double-U shaped welds were completed in about 8-10 passes (Figure 2). The weld metal in the welded specimens was taken from the outermost portion (surface) of the welds only. Weld microstructures are usually inhomogeneous by nature as discussed above. However, it is expected that the overall microstructure of the weld metal amongst the specimens used is similar since the filler metal and weld parameters were identical for all specimens, and because the outermost weld (the portion most affected this study) was carried out in only one pass. Since the welds had a double-U configuration, this meant that the volume of weld metal on the specimen was not the same throughout the ~2 mm thickness of the specimens. Nonetheless, the amount of weld metal in the specimens covered an area on the working surface that was at least 1 cm wide and extended across the entire face (perpendicular to the stem of the specimen) of the specimen on which the ceramic crevice formers (washers) were assembled. Thus, fully assembled, the MCA consisted of the Alloy 22 specimen (lollipop), one nut, one bolt, and two washers (all made of grade 2 Titanium (Ti)), as well as two ceramic crevice formers with multiple ridges. The bolts were polytetrafluoroethylene (PTFE) wrapped to prevent these hardware components from coming into electrical contact with the specimen. Each crevice former had a total of 12 ridges on it, creating 12 different potential crevice sites on each face of the specimen, and a total of 24 potential sites in each assembly (Figure 1). The bolt on the assembly was tightened to a torque of 70 in-lb. PTFE tape inserts were placed between the ceramic crevice formers and the MCA specimen (lollipop) on both sides prior to tightening. This was done to fill in the micro voids created by the micro-rough surfaces of the specimen and the ceramic crevice former, and to increase the reproducibly of the tight crevices in all specimens. The total surface area of the MCA specimen immersed in the electrolyte was 7.43 cm^2. This surface area included the area under the 24 ridges of the crevice formers, which had a combined surface area of 1.6 cm^2. In current density estimations, the surface area of 7.43 cm^2 was used for

calculations.

A three-electrode cell with a capacity of 1000 cm^3 was used for experimentation. The volume of electrolyte in the cell was ~900 cm^3. A saturated silver/silver chloride (SSC) (Ag/AgCl) electrode was the reference electrode (RE). The RE was maintained near room temperature by mounting it to the end of a Luggin probe, which had a water-cooled jacket around it. The temperature of the water pumped through the cooling jacket was between 5 and 12 °C. Thermal liquid junction calculations showed that potential variation caused by this phenomenon was in the order of a few mV (~10 mV maximum). Also, according to Macdonald et al., a high KCl concentration in the reference electrode tends to suppress thermal liquid junction potentials across the boundary between the high and low temperature solutions [30]. The liquid junction potential variations were therefore ignored in further analyses. The counter electrode was made of platinum (Pt) foil with a surface area of ~40 cm^2. The temperature of the electrolyte was maintained by means of an oil-filled heating bath. The specimen was immersed into the cell after the electrolyte had attained the desired temperature. This was done immediately after the grinding process. Solution temperature readings were taken before and after the experiment with a thermocouple. Electrochemical measurements were carried out with a potentiostat. The corrosion potential (E_{corr}) was monitored for 24 hours, which allowed E_{corr} to settle considerably. This was followed by cyclic potentiodynamic polarization measurements immediately afterwards. Both experiments were carried out in sequence on each test specimen. Cyclic polarization was started approximately 100 mV below E_{corr}, and continued until the current density from the specimen reached a maximum of up to 30 $mAcm^{-2}$, or a maximum of 1.3 V (SSC) before the scan was reversed. An upper limit of 30 $mAcm^{-2}$ was chosen because it was observed in previous experiments that anodic peaks with current densities as high as 20-30

$mAcm^{-2}$ could be generated on Alloy 22 in 5 M $CaCl_2$, especially between the temperatures of 60 and 75 °C [2]. The sweep rate in the forward and reverse directions was 0.1667 mVs^{-1} (600 mVh^{-1}). Deaerated 5 M $CaCl_2$ with a pH of ~5 was used in these experiments. Nitrogen gas (N_2) was bubbled through the electrolytes for at least one hour before and throughout the experiments at a rate of ~100 cc per minute. All electrolytes were prepared using certified American Chemical Society (ACS) reagent grade chemicals. In other experiments, potentiostatic polarization experiments were carried out for up to 24 hours in the same three-electrode configuration cell described above. The potentiostatic tested began immediately after the 24-hour corrosion potential (E_{corr}) monitoring period.

EXPERIMENTAL RESULTS

The Corrosion Potential (E_{corr})

Figure 3 shows a summary of the average E_{corr} values between 45 °C and 120 °C for wrought and welded specimens of Alloy 22. These are the averages from between 3 and 6 repeats. The error bars in Figure 3 are the standard deviations of the distributions. In each experiment, E_{corr} was recorded at the end of the 24-hour period of the experiments and used to compute the averages shown. Figure 3 shows that E_{corr} from the wrought and welded specimens can only be separated with confidence at 45 and 90 °C. They are statistically similar at all other temperatures as indicated by the overlapping error bars, although the welded specimen consistently registered higher mean values compared to the wrought specimens between 45 and 90 °C, and might indicate that the E_{corr} of the welded specimens are indeed higher, albeit by a slight margin within this temperature range. The E_{corr} of the wrought specimens was not affected by temperature.

The difference between the highest and lowest mean values of E_{corr} between 45 and 120 °C for wrought specimens was ~20 mV. However, the welded specimens were affected by temperature. The E_{corr} of welded specimens decreased with increase in temperature. There was a difference of ~120 mV between the highest and lowest mean E_{corr} values recorded on the welded specimens. Nonetheless, the E_{corr} values for the wrought and welded metals were relatively close over the entire range of temperature considered in these measurements (Figure 3).

The Breakdown Potential (E_b)

The breakdown potential, E_b, as employed here is used to denote the potential(s) at which the breakdown of the passive film occurs by any type of corrosion attack such as pitting corrosion, crevice corrosion, general dissolution, or transpassive dissolution.

Figures 4 and 5 show representative polarization curves at the extremes of the temperature range tested (45 and 120 °C) for the wrought and welded MCA specimens. At 45 °C, the curves for both the wrought and the welded Alloy 22 specimens showed a similar behavior, and overlap almost exactly. Under optical microscope examination, localized breakdown due to crevice corrosion was not observed on any of the specimens tested at 45°C on both the wrought and the welded specimens. The polarization curves of wrought and welded Alloy 22 specimens at 120 °C (Figure 5) were also similar. However, the welded specimen exhibited a higher breakdown potential compared with the wrought specimen. The polarization curves of the wrought specimens at 60, 75 and 90 °C were also similar to those collected from the welded specimens at the corresponding temperatures. The polarization curves at 90 °C were similar to those at 120 °C. At 60 and 75 °C however, the shape of the curves, and thus the electrochemical behavior of Alloy 22 differed from the behavior at temperatures of 90 and 120 °C (Figure 6).

In Figure 6, there is a drop in current density after an initial rise in current density from the passive region at 60 and 75 °C. This drop in current density created an "anodic peak" or "hump" usually between 0.0 and 0.5 V_{SSC}. The peaks from specimens at 75 °C were broader and had higher peak current densities than those at 60 °C. These current excursions sometimes reached values of about 20-30 $mAcm^{-2}$ at 75 °C. After the anodic peak or hump, there is a secondary passive region. The current density of the secondary passive region was higher than that of the primary passive region. The current density of the secondary passive region at 75 °C was much greater than that at 60 °C. Beyond the secondary passive region, transpassive dissolution resulted on further increase of the applied potential. At 60 °C the current density in the secondary passive regions was usually low enough to represent true repassivation of the surface (Figure 6). However, due to the relatively high current density in the secondary "passive" regions at 75 °C, it is unlikely the current densities as high as those shown in Figure 6 at 75 °C represent true passivity.

Upon inspection with an optical microscope, only localized (crevice) corrosion was observed on specimens (at 60 °C) where the potential was reversed at or near the peak current density in the anodic peak (hump). Where the experiments proceeded to potentials corresponding to regions of transpassive dissolution (at 60 and 75 °C), two types of damage were observed on the specimens; localized corrosion, which commenced at potentials corresponding to the beginning of the anodic peak or hump, and general dissolution due to transpassivation, which occurred at much higher potentials after the repassivation of the anodic peak. As observed in Figure 6, no hystereses loop occurred (at 60 nor at 75 °C) when the potential reached the higher values corresponding to the transpassive region of Alloy 22.

Not all the wrought specimens tested at 60 °C exhibited the hump. In addition, none of the three welded specimens tested at 60 °C exhibited the hump. In these specimens, only transpassive dissolution was observed when the specimens were inspected under the optical microscope. This is consistent with the absence of hystereses loops at the elevated potentials where the applied potential was reversed. The reasons for presence or absence of the hump in these specimens are not fully understood.

Figure 7 shows a summary of the breakdown potentials (E_b) and the repassivation potential (E_{rp}) for both the wrought and the welded specimens. These data points are from an average of at least 2 data values. The error bars are standard deviations of the distribution. E_{corr} values have been included for easy comparison with E_b and E_{rp}. The method used to determine E_b was the current density inflection (of the curve) method. In this method, E_b is the potential at which a permanent rise in current density from the passive region commences. In most cases, E_b was easily determined due to the abrupt increase in current from passive region, indicative of the onset of localized breakdown (Figure 5). At 60 and 75 °C where anodic peaks or "humps" occur, E_b was taken as the potential at the base (beginning) of the "hump". Specimens held at a potential (~0.325 V_{SSC}) corresponding to the peak current density in the hump at 75 °C (Figure 6) in potentiostatic polarization experiments for up to 24 hours showed that the specimens did not passivate. In fact, there was massive dissolution of the metal hence the potential at the base of the hump where the current density started to rise was taken as E_b. Figure 8 shows about 70,000 s of the current and current density transients from a potentiostatic experiment performed at 75 °C. The abrupt fall in current and current density at about 67 000s coincides with the detachment of the crevice assembly (remnant of the lollipop head, ceramic and titanium (Ti) washers, Ti as well as bolt and nut) from the stem of the specimen (Figure 1). The current

registered after the abrupt fall is from the portion of the stem of the specimen still in contact with the electrolyte.

E_b decreased steadily with increase in temperature between 45 and 120 °C (Figure 7). Since localized breakdown was not observed under optical microscopy at 45 °C on both the wrought and the welded specimens, E_b was attributed to transpassive dissolution and not localized breakdown. No localized corrosion was observed at 60 °C on the welded specimens, but was observed on the wrought metal at this temperature. At 75 °C and above, E_b represented localized breakdown due to crevice corrosion on both the wrought and welded specimens. The E_b of the wrought and welded specimens at 75 and 90 °C were difficult to separate statistically since the error bars overlapped. However, at 120 °C, E_b was higher on the welded specimens, and hence more resistant to localized (crevice) corrosion compared with the wrought specimens.

The degree of damage due to localized corrosion increased with temperature. The crevices formed at 60 °C were the shallowest and caused the least damage per unit area. Crevice corrosion was virtually non-existent in the weld metal zone in welded specimens (Figures 9 and 10). Where it occurred, it was less severe than in the crevices in the base metal zone. In Figure 9 (75 °C; 5 M $CaCl_2$), the band of weld metal appears darker than the base metal zone in the top portion of the photo. The deepest crevices were located in the base metal zone. Similarly, in Figure 10 (120 °C, 5 M $CaCl_2$), the deep crevices that formed in the lower base-metal half of the image terminate at the boundary of the base and weld metal. In Figure 10, the weld metal zone deflects the growth path of the crevices away from itself (the weld zone), thus confining crevice damage to the base metal zone. These images imply that the weld metal is significantly better able to resist localized attack in 5 M $CaCl_2$ in spite of the similarities in the E_b of the wrought and welded specimens especially at 75 and 90 °C.

The Repassivation Potential (E_{rp})

Two methods were used to measure the repassivation potential for localized corrosion, E_{rp}. In the first method, the repassivation potential was the potential that coincided with a current density of 1 μAcm^{-2} (1×10^{-6} Acm^{-2}) on the reverse sweep of the cyclic polarization curves. "E_{rp1}" in Figure 7 denotes the values obtained in this fashion. In the second method, denoted by "E_{rp2}" (Figure 7), the repassivation potential was the potential that coincided with the point where the reverse and forward sweeps of the polarization curve intersected. Figure 7 shows that comparable values of E_{rp} are obtained from these two methods, as exemplified in the similarities of E_{rp1} and E_{rp2} values. In fact, at 75, 90 and 120 °C, the values were statistically indistinguishable because of the overlap of the data points as well as the error bars. There are no E_{rp} values for the wrought and welded specimens at 45 °C, and for the welded specimens at 60 °C since there was no localized corrosion observed on the specimens at these temperatures. It should be noted that because of the repassvation of the specimens (after the occurrence of the anodic peak), the repassivation potentials measured cannot be sole attributed the occurrence of localized corrosion, but to transpassive dissolution.

There is a difference of at least 240 mV_{SSC} between E_b and E_{rp} in the wrought and the welded specimens, with E_{rp} being the lower potential as expected. E_{rp} decreased with increasing temperature, just as E_b did. The E_{rp} values were similar for both the wrought and the welded specimens, even at 120 °C where E_b was distinctly higher on the welded specimens. All E_{rp} values were higher than the corresponding E_{corr} values (Figure 7). Therefore, to attain localized corrosion of Alloy 22 in pure 5 M $CaCl_2$ solution, polarization above E_{corr} is required.

DISCUSSION

The similarity in the values of the E_{corr} (except at 45 and 90 °C) for the wrought and the welded specimens over the temperature range tested suggest that there might be difficulty in creating and sustaining viable galvanic couples which could lead to localized breakdown of the oxide film either on the base metal or weld (depending on which potential is higher). This suggest that the possibility of localized corrosion occurring due to a galvanic couple (between weld and base metal) either on the weld or base metal under open circuit conditions in 5 M $CaCl_2$ is remote. One possibility is that since the compositions of the wrought and filler metal used for the specimens are very similar, the expectation is that the nominal composition of the final weld metal would be similar to that of the weld filler metal and wrought portions of the specimens (Table 1), and hence the similarity in the E_{corr} values. Another possibility is that due to the fact that alloys like 625 and 22 usually suffer less from the effects of microsegregation compared with more lightly alloyed Ni-alloys [13, 15, 16], any E_{corr} variations between the welded and wrought specimens arising from microsegregation were likely ameliorated or suppressed by the high alloy content of Alloy 22.

The E_{corr} values recorded for the welded specimens are in reality, a composite of the welded and wrought materials. A slight difficulty therefore arises in accurately separating the contribution by the welded and wrought portions of the welded specimens. Nonetheless, although the E_{corr} of the welded specimen is a composite of the E_{corr} of the weld and base metals, the closeness of the E_{corr} of the pure base and welded specimens strongly suggests that the E_{corr} of pure base metal (wrought) might be close to that of pure weld metal.

A limitation of the method used in the determination of E_b is that it is not always able to give the exact potential at which localized breakdown commences. This is because the current values being monitored for localized corrosion are composites of the passive current density and that due to localized corrosion. Therefore, in order for a current rise (over and above the passive (background) current) to be observed, the localized corrosion event would need to grow to such a size that would enable it to put out a current higher than that of the passive current of the specimen. The amount of growth that is required would depend on how large the surface of the specimen is since it scales directly with the value of the background current. Generally, the smaller the specimen, the earlier the current due to localized breakdown will be detected, and the closer the determined E_b will be to the actual potential at which localized breakdown commenced [31]. However, increasingly smaller specimens lead to elevated E_b values, as the number of potential sites for the nucleation of localized events reduces with size [31]. Other methods like the current threshold method, in which a current or current density is used to determine the onset of localized corrosion is also froth with uncertainties with regard to determining the exact onset of localized corrosion. Too low a threshold current value will lead to E_b values in the regions where the specimen is still passive. Too high a threshold value leads to E_b values that are artificially high. Consequently, the current threshold method is best employed only as a basis for comparison amongst systems. The E_b values as used in this work represent a basis for comparison. No absolute values are implied for use to make predictions.

The similar values of E_b obtained at 75 and 90 °C from the wrought specimens, and higher values obtained at 120 °C for the welded specimens of Alloy 22 in 5 M $CaCl_2$ suggest that in this environment, GTAW welds did not cause any adverse effect on the resistance of Alloy 22 to localized corrosion under the present test conditions. The images in Figure 9 and 10 suggest that the weld and base (wrought) metals exhibit different propensities to crevice corrosion, with the

weld metal able to better resist crevice corrosion. Since the welded specimens do not contain pure weld metal, the values of E_b presented for both the welded specimens might therefore reflect the E_b of the base metal in the specimen, rather than that of the weld metal alone which might be much higher in reality. The greater susceptibility of the base compared with the weld metal is believed to be due to metallurgical effects. Pure base and pure weld metals are required to understand, and possibly isolate the main reason(s) for the differences in susceptibility to localized corrosion, and to compute the true contribution of each potion of the welded specimen to the final E_b values realized in these experiments.

A very important point from this study is that with regard to the welds, it appears that no detrimental effects on crevice corrosion resistance resulted from the presence of secondary phase or carbide precipitates, or other elemental segregation (especially of Mo) in the dendritic and interdendritic regions, or from the microstructure. The enrichment of Mo in the secondary phases and the interdendritic regions usually results in the depletion of Mo form the adjacent matrix and result in the formation of favored sites for localized corrosion initiation. Analyses carried out by other workers at LLNL on the same batch of welds as used for specimens in this work showed that the volume fraction of TCP phases present in this welds was about 0.10% [32]. The TCP phases consisted of predominantly P and μ [32]. This finding is consistent with the findings of other workers [33]. One reason for the resistance of these welds to crevice corrosion in 5 M $CaCl_2$ is that as suggested by Leonard et al. [17], the number of precipitate particles which, constitutes this small volume fraction of TCP phases was not sufficient enough to induce preferential localized attack in the welds. However, one might also suspect that if these particles fall below a certain threshold in size, and are dispersed, they might not be able to act as sites for the initiation of stable localized corrosion. It is also reasonable to assume that if there were other

unidentified precipitates or intermetallic compounds in the welds, they did not compromise the localized corrosion resistance of the welds.

The anodic peaks or "humps" exhibited by both the base and the welded versions of the specimens at 60, and 75 °C are associated with localized attack that either passivated (at 60 °C) or was stifled (at 75 °C) upon an increase in potential. In addition, there is some difficulty in reactivating the sites of localized breakdown after passivation (at 60 °C) had occurred. The reason why passivation took place after initial breakdown is not fully understood. However, potentiostatic polarization experiments carried out at potentials equivalent to the maximum current density in the anodic peak showed that the high current densities were sustained throughout the experiment (Figure 8), despite the slight fall in these current densities with time. Therefore, it appears that the repassivation on the forward sweep of the polarization was associated with the increase in potential.

The close proximity of the E_{rp1} and E_{rp2} shows that identical results are realized on Alloy 22 in the systems tested by these two measurement techniques (Figure 7). Further, Figure 7 shows that welding employed in this study does did not adversely affect recovery from crevice breakdown. However, this is not surprising since the areas of most severe attack were predominantly in the base metal portion of the specimens.

CONCLUSIONS

1. After 24 hours of exposure to 5 M $CaCl_2$, the E_{corr} of the wrought MCA Alloy 22 is not affected by temperature between 45 and 120°C. However, after 24 hours of

exposure to 5 M $CaCl_2$, the E_{corr} of the welded MCA specimens of Alloy 22 decreases ~120mV with increase in temperature between 45 and 120 °C.

2. During anodic potentiodynamic polarization, localized corrosion was observed on wrought specimens at 60 °C and above, and at 75 °C and above for the welded in 5 M $CaCl_2$. No localized corrosion was observed at 45 °C on both the wrought and welded specimens, and at 60 °C on the welded specimens in 5 M $CaCl_2$.
3. E_b shifted to lower potentials as temperature increased on both the wrought and welded specimens in 5 M $CaCl_2$.
4. E_b was similar on the wrought and welded specimens at 75 and 90°C but was lower on the wrought specimens at 120 °C in 5 M $CaCl_2$.
5. The weld metal was found to be less susceptible to crevice attack compared with the base metal in the welded specimens in 5 M $CaCl_2$.
6. Where localized corrosion occurred, the E_{rp} was similar on both the wrought and the welded specimens in 5 M $CaCl_2$.
7. E_{rp} decreased with increase in temperature on the wrought and welded specimens in 5 M $CaCl_2$.

REFERENCES

1. G.O. Ilevbare, T. Lian and J.C. Farmer, Environmental Considerations in the Studies of Corrosion Resistant Alloys for High-Level Radioactive Waste Containment Paper No. 02539, Corrosion 2002.

2. G.O. Ilevbare, Electrochemical Behavior of Alloy 22 in 5 M $CaCl_2$, Transportation Storage, and Disposal of Radioactive Materials, PVP-Vol. 449, p.55 2002. American Society of Mechanical Engineers (ASME), New York, USA.

3. B. A. Kehler, G.O. Ilevbare and J.R. Scully, Corrosion, **57**, 1042 (2001).

4. B. A. Kehler, G. O. Ilevbare and J. R. Scully, Corrosion 2001, Crevice Corrosion Behavior, of Ni-Cr-Mo Alloys: Comparison of Alloys 625 and 22, NACE Topical Research Symposium, p.30, March 2001.

5. Haynes International, Inc., Product Brochure H-2019E, Haynes International Inc. Kokomo, IN, p.22, 1997.

6. J. C. Farmer, D. McCright, G.E. Gdowski, F. Fang, T. Summers, P. Bedrossian, J. Horn, T. Lian, J. Estill, A. Lingenfelter, and W. Halsey, General and Localized Corrosion of Outer Barrier of High-Level Waste Container in Yucca Mountain, May 2000. Preprint UCRL-JC-138890, Lawrence Livermore National Laboratory, Technical Information Department Digital Library.

7. K.A. Gruss, G.A. Cragnolino, D.S. Dunn and N.Sridhar, Corrosion '98, Paper No. 149, 1998.

8. S.J. Lukezich, The Corrosion Behavior of Ni-Base High Performance Alloys in Simulated Repository Environments, MS Thesis, The Ohio State University 1989.

9. N.J. Laycock,V.M. Linton, P.T. Wilson, M.P. Ryan and D.S. Crouch, Proceedings of the International. Institute of Welding (IIW) Asian Pacific Welding Congress, NZIW 2000 annual Conference and) 48th Annual Conference of the Welding Technology Institute of Australia (WTIA) Melbourne, Australia, Vol. 2, Paper 87, 2000.

10. E. Smailos, Corrosion, **59**, 1071 (2000).

11. K Ogawa M Miuar and T. Minami, Transactions of the Japan Welding Society, **21**, 52 (1990).

12. J.B Hill and A.H. Tuthill, In Pulp and Paper Industry Corrosion Problems. Proceedings of the 4th International Symposium, Stockholm Sweden 1983, p 142-148

13. A.H. Tuthill and R.E. Avery, Supplement to the Welding Journal, February, p. 41-s (1993).

14. A. Garner, Materials Performance, **21**, 9 (1982).

15. L.S. Redmerski, J.J. Eckenrod and C.W. Kovach, Materials Performance, **22** No. 1, 31 (1983).

16. P. Woolin, Proceedings of the Stainless Steel World conference 1999, The Hague Netherlands paper SSW99-033 pg 111 Book 1

17. A.J. Leonard, P. Woolin and D.C. Buxton, Proceedings of the Stainless Steel World conference 2001, The Hague Netherlands, 13-15 November 2001 Paper No. P0185

18. V.N. Lipodaev, K.A. Yuschenko and Y.U. Sidorkina, Automatic Welding, **30**, 46 (1983).

19. L.H. Flasche and I.J. Storey, Weld Failures, Proceedings, International Conference London 21-24 Nov 1988, Ed., J.D. Harrison, Paper 41 p.275-293 (1989).

20. T.P.S. Gill, Proc. Int. Conf. On Corrosion CONCORN' 97 December 3-6 Mumbai India p.398 (1997).

21. L Garverick (Editor), In Corrosion of Weldments in Corrosion in the Petrochemical Industry Editor L Garverick, p 126-160, ASM International 1994.

22. S.D. Kiser and C. Cooper, International Institute of Welding (IIW) Asian Pacific International Congress. Proceedings, Conference, Singapore, 29 Oct.-1 Nov.2002. Publ: Lidcombe, NSW 2141, Australia; Welding Technology Institute of Australia (WTIA); 2002. ISBN 0-909539-99-5. Vol.1-2. Paper 12. 12pp.

23. A.J. Smith, R.P. Stratton and B Tuttle, Proceedings of the Sixth International Symposium on Environmental Degradation of Materials in Nuclear Power Systems, San Diego California, 1-5 August 1993 p. 97.

24. A. Garner, Corrosion, **35**, 108 (1979).

25. M.J. Cieslak, T.J. Headley and A.D. Romig Jr, Metallurgical Transactions A, **17A**, 2035, (1986).

26. J.R. Crum, E.L. Hibner and R.W. Ross Jr., Materials Performance, **20**, 9 (1981).

27. http://cst-www.nrl.navy.mil/lattice/struk/laves.html

28. ASTM B574, Annual Book of ASTM Standards, Nonferrous Metal Products, Volume 02.04, p.531, American Society of Testing and Materials, West Conshohocken, PA (2000).

29. ASTM B575, Annual Book of ASTM Standards, Nonferrous Metal Products, Volume 02.04, p.535, American Society of Testing and Materials, West Conshohocken, PA (2000).

30. D.D. Macdonald, A.C. Scott, and P. Wentrcek, J. Electrochem. Soc., **126**, 908 (1978).

31. G.T Burstein and G. O. Ilevbare, in Corrosion Science, **38**, 2257 (1996).

32. B. S. El-Dasher and S. G. Torres, TMS Letters, Effect of Stress Mitigation on Precipitation of Alloy 22 Welds (2005). (Page numbers and volume of citation yet to be assigned by TMS).

33. Y.-M. Pan, D.S. Dunn, and G.A. Cragnolino, Metallurgical and Materials Transactions A, **36A**, 1143, (2005).

Acknowledgements

The Department of Energy Office of Civilian Radioactive Waste Management (OCRWM) sponsored this work. This work was done under the auspices of the U.S. Department of Energy (DOE) by the University of California, Lawrence Livermore National Laboratory (LLNL) under contract No. W-7405-Eng-48. This work is supported by the DOE Office of Repository Development, LLNL.

Table 1. Chemical composition of Alloy 22 (UNS No. N06022) given in weight percent.

Element	Actual Composition		
	Wrought	Welded (Weld/Filler Metal)	Welded (Base Metal)
Mo	14.10	14.00	13.82
Cr	22.00	20.54	20.38
Fe	4.50	2.08	2.85
W	2.70	3.10	2.64
Co	1.30	0.03	0.01
C	0.003	0.004	0.005
Si	0.03	0.06	0.05
Mn	0.31	0.20	0.16
V	0.16	0.03	0.171
P	0.01	0.004	0.008
S	<0.01	0.001	0.0002
Ni	Bal.	Bal.	Bal

Wrought Specimens from Heat # 2277-5-3203. Welded Specimens: Base metal from Heat #059902LL1; Weld/filler metal from Heat # XX1753BG inco international.

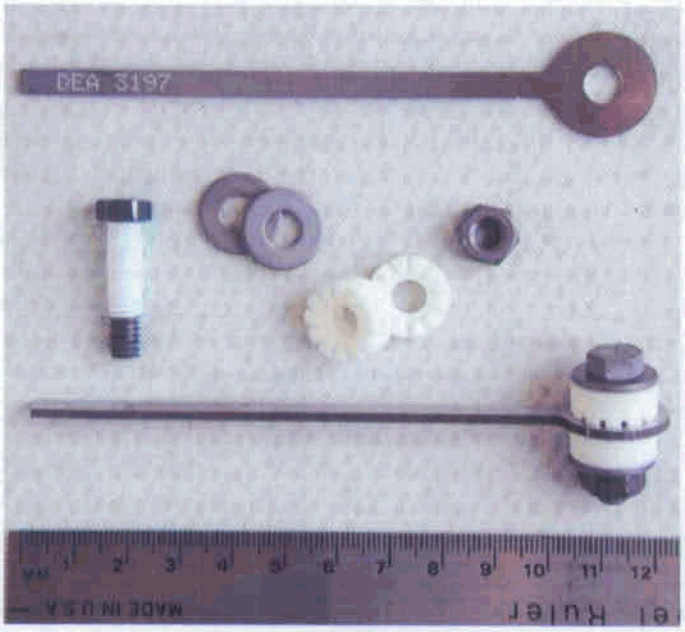

Figure 1: Multiple Crevice Assembly (MCA), bottom. It shows the lollipop-like specimen (top), titanium grade two bolt (Teflon wrapped for electrical insulation), washers nut and ceramic washers.

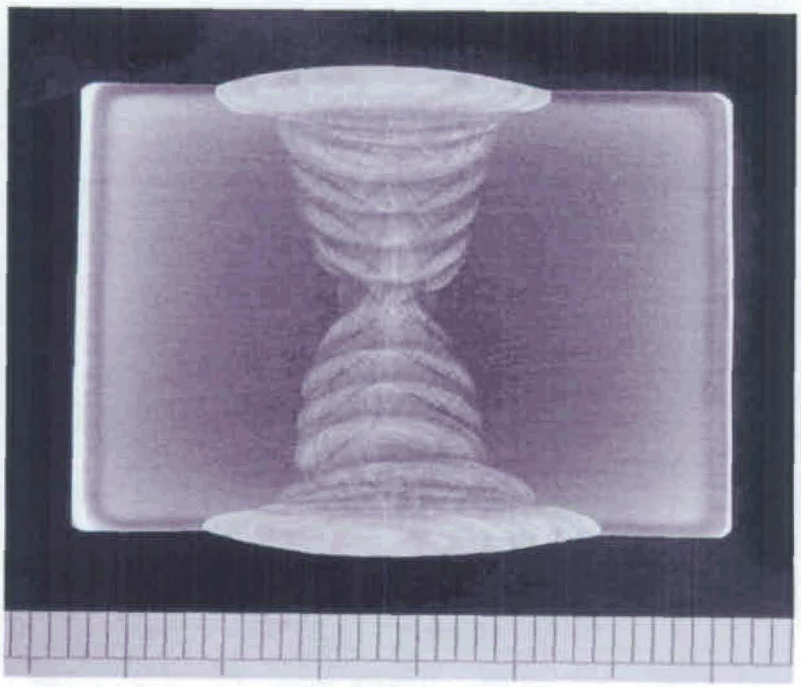

Figure 2: Cross-section of welded plate from which welded MCA specimens were fabricated. Double-U weld was completed in 8-10 passes. The plate is 3.175 cm (1.25 inches) thick.

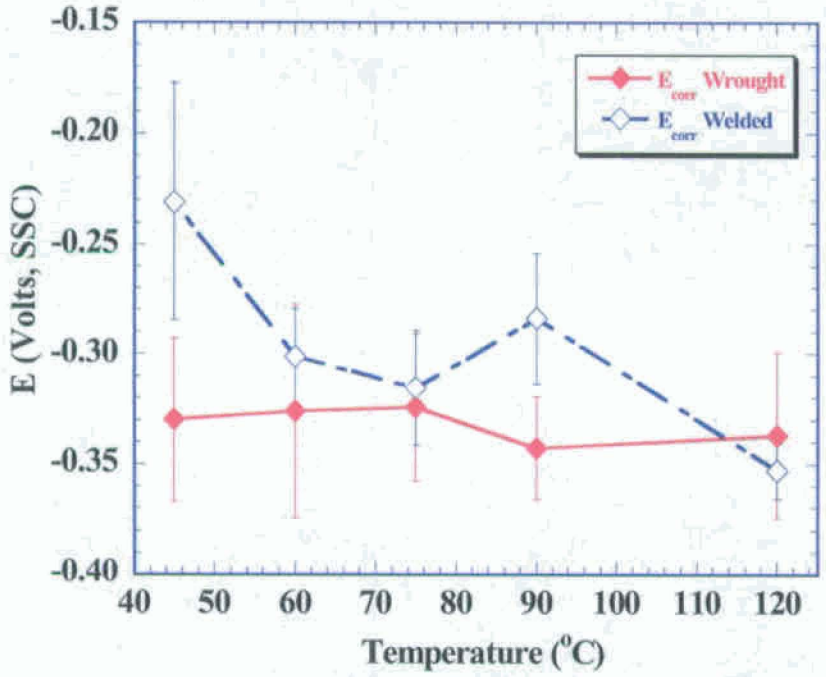

Figure 3: E_{corr} as a function of temperature on wrought and welded MCA specimens in 5 M $CaCl_2$. E_{corr} was measured after 24 hour of immersion in solution.

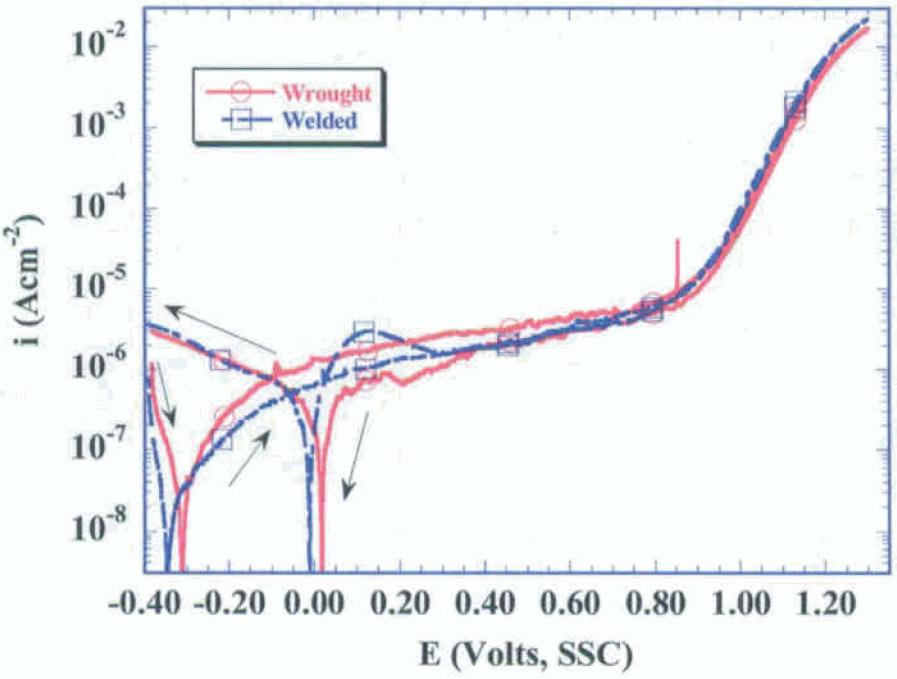

Figure 4: Polarization curves of wrought and welded MCA specimens in 5 M $CaCl_2$ at 45 °C. Sweep rate, 0.1667mV/s.

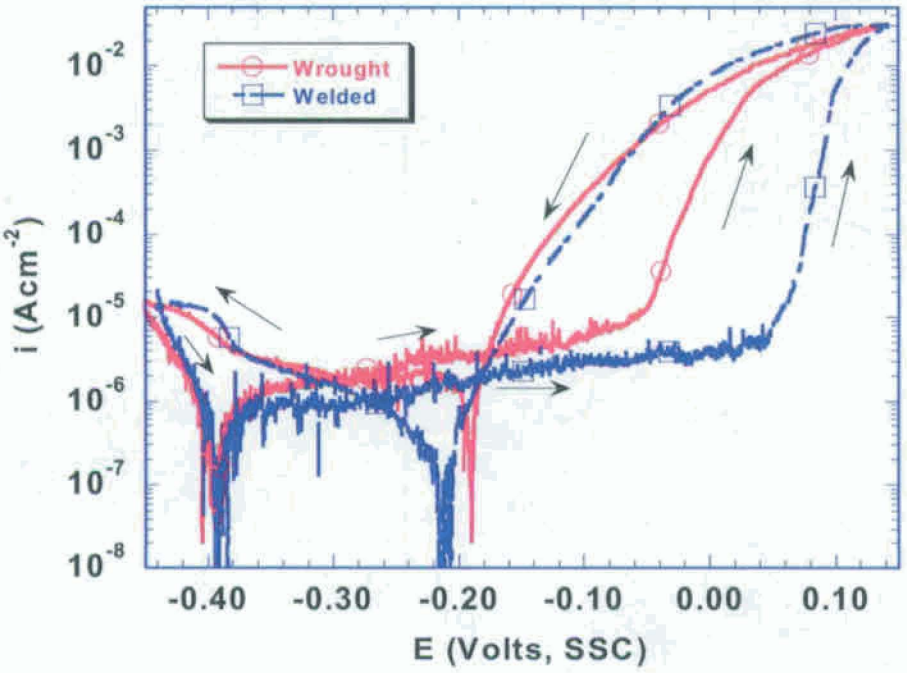

Figure 5: Polarization curves of wrought and welded MCA specimens in 5 M $CaCl_2$ at 120 °C. Sweep rate, 0.1667mV/s

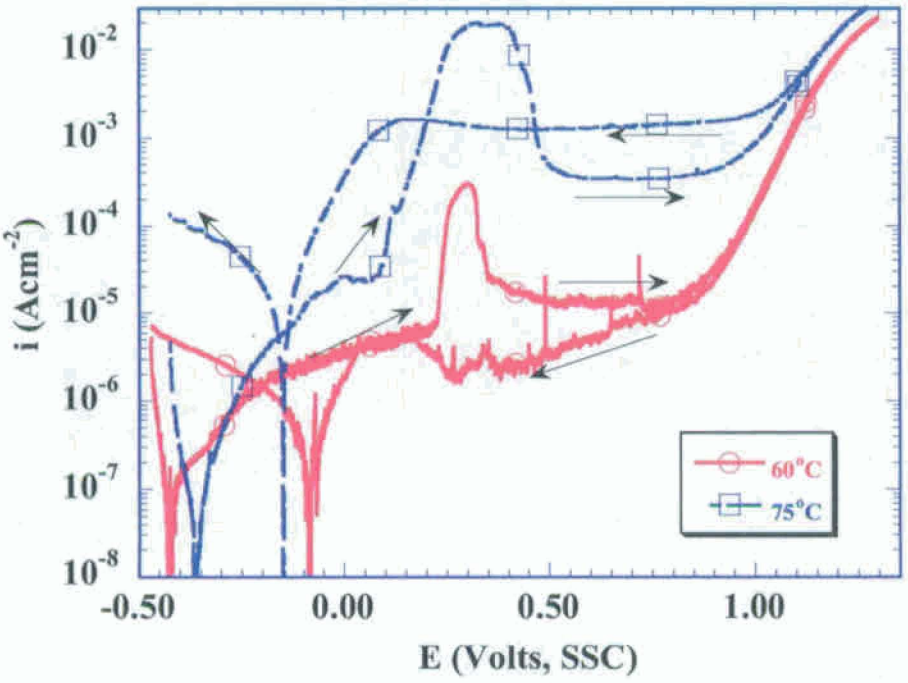

Figure 6: Polarization curves of wrought MCA specimens in 5 M $CaCl_2$ at 60 and 75 °C. Sweep rate, 0.1667mV/s

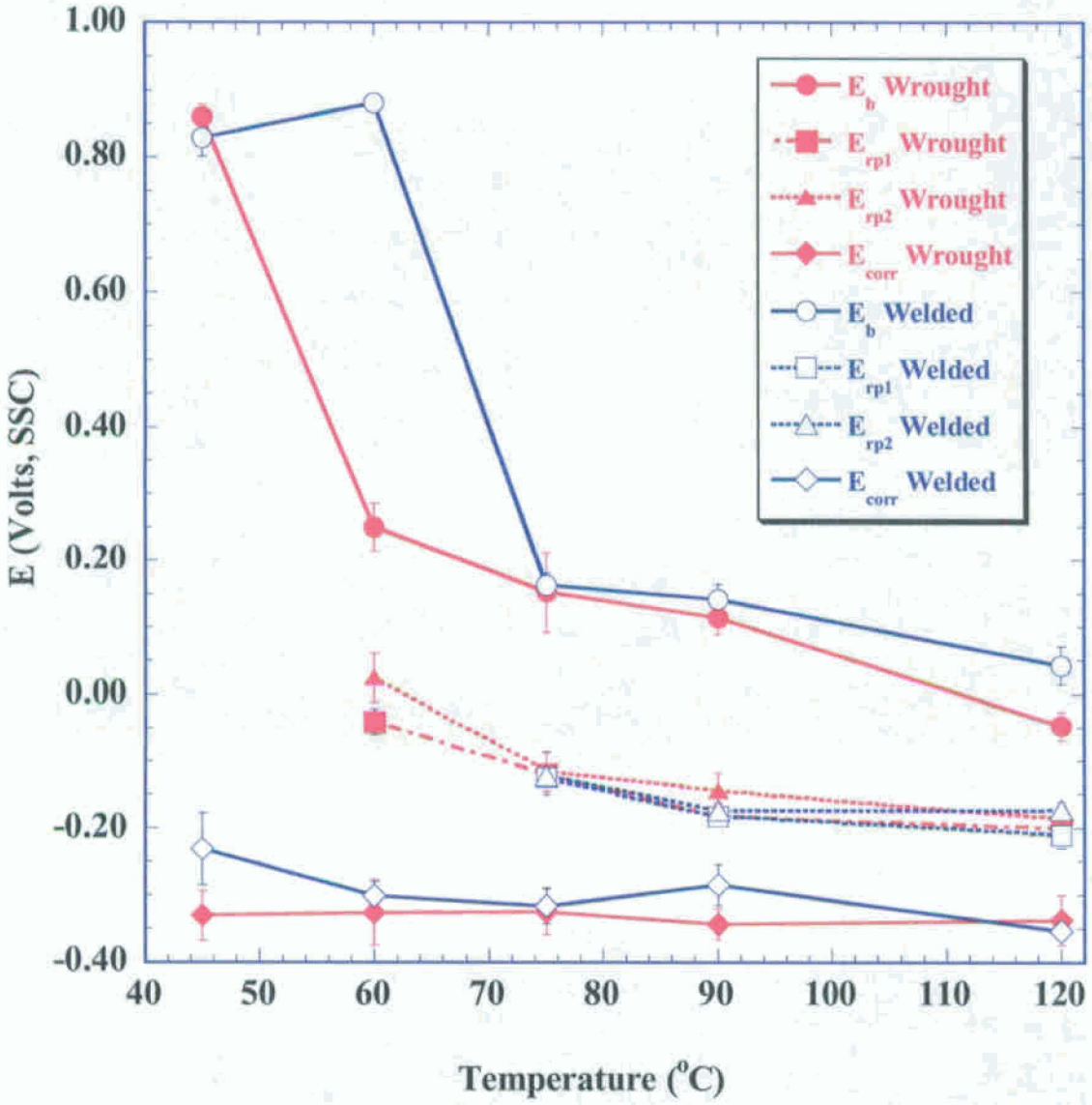

Figure 7: Average critical potential for breakdown, E_b, the repassivation potential E_{rp}, and the corrosion potential E_{corr}, as a function of temperature on wrought and welded MCA Alloy 22 specimens in 5 M $CaCl_2$. E_{rp1} is the potential at which the threshold current density of 1×10^{-6} Acm^{-2} was reached on the reverse sweep of the polarization curve. E_{rp2} is the potential at which the reverse and forward sweeps of the polarization curve intersect.

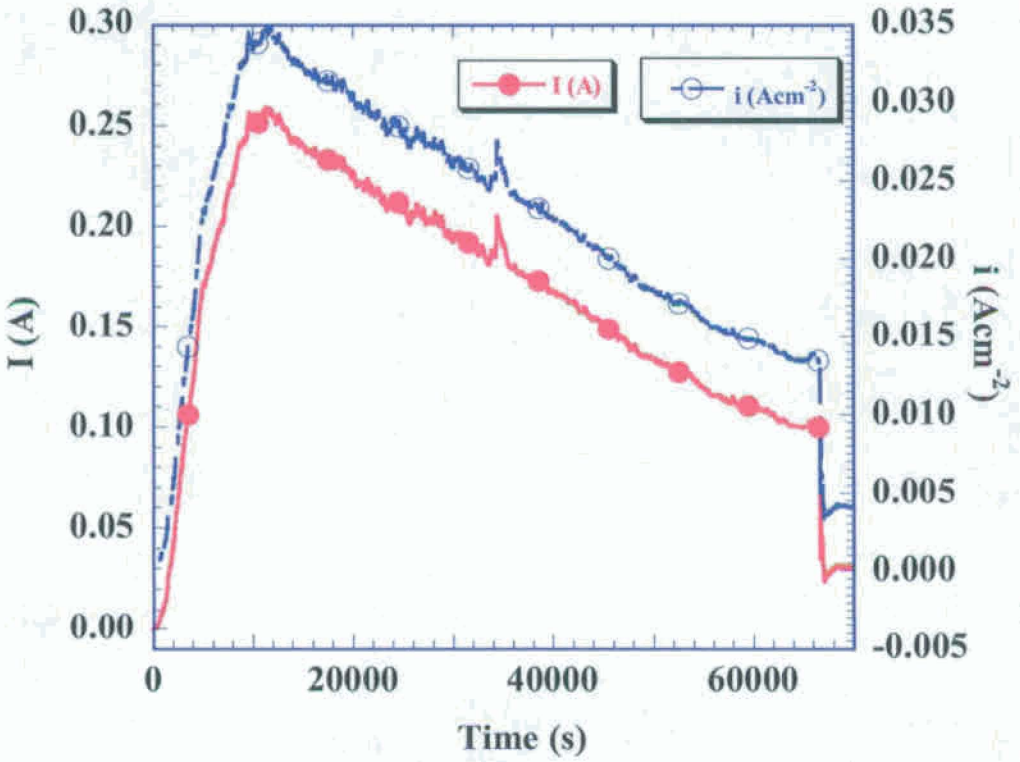

Figure 8: Current and current density transients of wrought MCA Alloy 22 at 0.325 V (SSC). These transients show 70 000s of the transient. The abrupt fall in current and current density at about 67 000s possibly coincides with the detachment of the lollipop head from the stem of the specimen (See Figure 1).

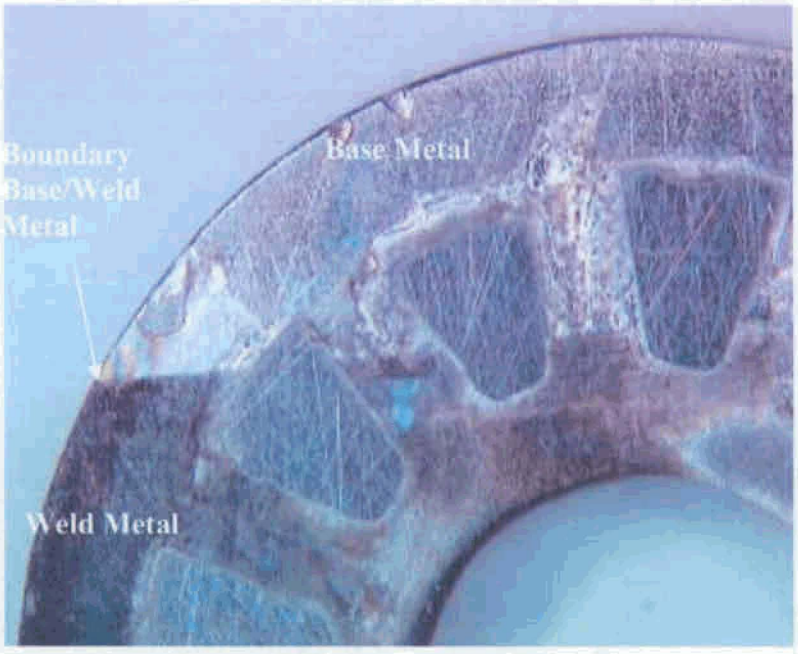

Figure 9: Welded MCA after 24 hours at E_{corr}, and cyclic polarization in 5 M $CaCl_2$ at 75 °C. The attack in this case follows the perimeter of individual crevice teeth and terminates in each case at the boundary of the base/weld metal.

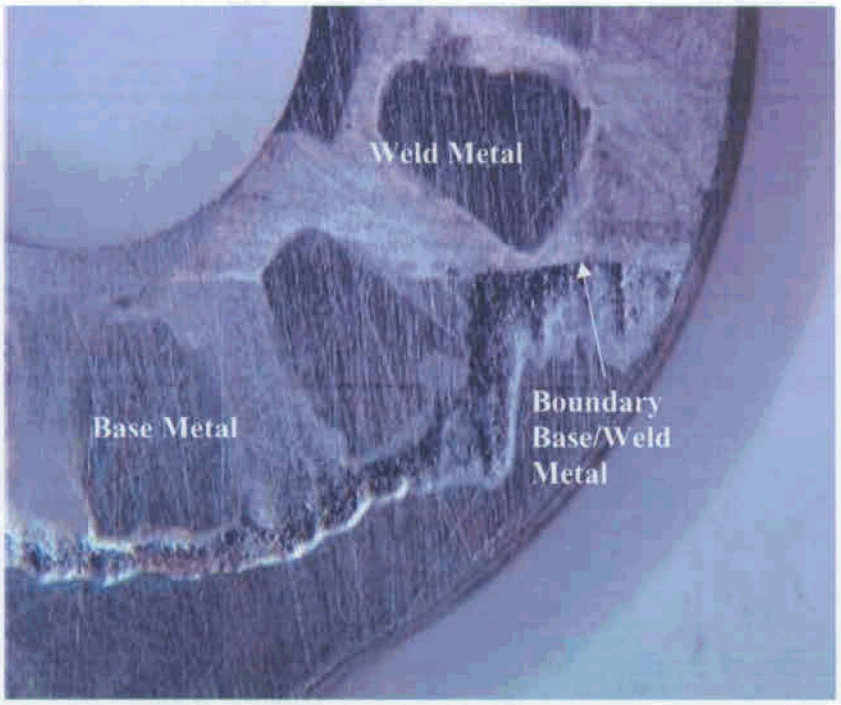

Figure 10: Welded MCA after 24 hours at E_{corr}, and cyclic polarization in 5 M $CaCl_2$ at 120 °C. In this case the attack follows the perimeter of the entire crevice former but terminates at the base/weld metal boundary.

List of Figure Captions

Figure 1: Multiple Crevice Assembly (MCA), bottom. It shows the lollipop-like specimen (top), titanium grade two bolt (Teflon wrapped for electrical insulation), washers nut and ceramic washers.

Figure 2: Cross-section of welded plate from which welded MCA specimens were fabricated. Double-U weld was completed in 8-10 passes. The plate is 3.175 cm (1.25 inches) thick.

Figure 3: E_{corr} as a function of temperature on wrought and welded MCA specimens in 5 M $CaCl_2$. E_{corr} was measured after 24 hour of immersion in solution.

Figure 4: Polarization curves of wrought and welded MCA specimens in 5 M $CaCl_2$ at 45 °C. Sweep rate, 0.1667mV/s.

Figure 5: Polarization curves of wrought and welded MCA specimens in 5 M $CaCl_2$ at 120 °C. Sweep rate, 0.1667mV/s.

Figure 6: Polarization curves of wrought MCA specimens in 5 M $CaCl_2$ at 60 and 75 °C. Sweep rate, 0.1667mV/s

Figure 7: Average critical potential for breakdown, E_b, the repassivation potential E_{rp}, and the corrosion potential E_{corr}, as a function of temperature on wrought and welded MCA Alloy 22 specimens in 5 M $CaCl_2$. E_{rp1} is the potential at which the threshold current density of 1×10^{-6} Acm^{-2} was reached on the reverse sweep of the polarization curve. E_{rp2} is the potential at which the reverse and forward sweeps of the polarization curve intersect.

Figure 8: Current and current density transients of wrought MCA Alloy 22 at 0.325 V (SSC). These transients show 70 000s of the transient. The abrupt fall in current and current density at about 67 000s possibly coincides with the detachment of the lollipop head from the stem of the specimen (See Figure 1).

Figure 9: Welded MCA after 24 hours at E_{corr}, and cyclic polarization in 5 M $CaCl_2$ at 75 °C.

Figure 10: Welded MCA after 24 hours at E_{corr}, and cyclic polarization in 5 M $CaCl_2$ at 120 °C.